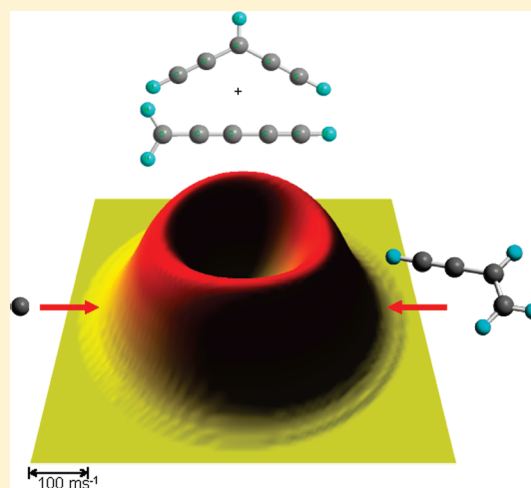


# On the Formation of Resonantly Stabilized C<sub>5</sub>H<sub>3</sub> Radicals—A Crossed Beam and Ab Initio Study of the Reaction of Ground State Carbon Atoms with Vinylacetylene

Dorian S. N. Parker,<sup>†</sup> Fangtong Zhang,<sup>†</sup> Y. Seol Kim,<sup>†</sup> and Ralf I. Kaiser<sup>\*,†</sup><sup>†</sup>Department of Chemistry, University of Hawaii at Manoa, Honolulu, HawaiiAlexander M. Mebel<sup>‡</sup><sup>‡</sup>Department of Chemistry and Biochemistry, Florida International University, Miami, Florida Supporting Information

**ABSTRACT:** The formation of polycyclic aromatic hydrocarbons in combustion environments is linked to resonance stabilized free radicals. Here, we investigated the reaction dynamics of ground state carbon atoms, C(<sup>3</sup>P<sub>1</sub>), with vinylacetylene at two collision energies of 18.8 kJ mol<sup>-1</sup> and 26.4 kJ mol<sup>-1</sup> employing the crossed molecular beam technique leading to two resonantly stabilized free radicals. The reaction was found to be governed by indirect scattering dynamics and to proceed without an entrance barrier through a long-lived collision complex to reach the products, *n*- and *i*-C<sub>5</sub>H<sub>3</sub> isomers via tight exit transition states. The reaction pathway taken is dependent on whether the carbon atom attacks the π electron density of the double or triple bond, both routes have been compared to the reactions of atomic carbon with ethylene and acetylene. Electronic structure/statistical theory calculations determined the product branching ratio to be 2:3 between the *n*- and *i*-C<sub>5</sub>H<sub>3</sub> isomers.



## 1. INTRODUCTION

The formation of polycyclic aromatic hydrocarbons (PAHs) and related species such as their cations, anions, as well as partially hydrogenated and dehydrogenated counterparts has been the subject of investigation by both the astrochemistry and combustion communities for over four decades. In terrestrial environments, the formation of PAHs and soot particles is thought to be linked and to proceed stepwise via small radicals such as propargyl (C<sub>3</sub>H<sub>3</sub>), which are often resonantly stabilized.<sup>1–3</sup> Most importantly, soot emissions in combustion processes<sup>4–7</sup> present significant health risks due to their carcinogenic properties<sup>8,9</sup> and possible role in the degradation of atmospheric ozone.<sup>10</sup> A reduction and, ultimately, elimination of the formation of soot would therefore provide cleaner and more efficient combustion systems and eliminate the associated health risks. Whereas on Earth, PAHs and soot particles are unwanted byproducts, these species contribute significantly to the astrochemical evolution of the interstellar medium (ISM). Here, the formation of PAHs is linked to the synthesis of hydrogen-deficient, small hydrocarbon molecules in interstellar clouds<sup>11,12</sup> and also in atmospheres of planets and their moons, such as Saturn's satellite Titan.<sup>13,14</sup> The

haze layers of Titan, which control the moon's weather pattern and radiation balance (green house effect), are indicative of a process of cycling from gaseous molecular hydrocarbons to particulate matter<sup>13,14</sup> involving PAH-like species.

Resonantly stabilized hydrocarbon radicals, such as the C<sub>2v</sub> symmetric propargyl radical (H<sub>2</sub>CCCH),<sup>15</sup> in which the unpaired electron is delocalized and spread out over three carbon atoms in the molecule, has received considerable attention in its role as a reaction intermediate to form PAHs. The delocalization of the unpaired electron results in a number of resonant electronic structures of comparable importance. Owing to the delocalization, resonantly stabilized free hydrocarbon radicals (RSFRs) are more stable than ordinary radicals.<sup>15</sup> Consequently, RSFRs can reach high concentrations in flames. These high concentrations make them important reactants to be involved in the formation of soot and PAHs, such as the formation of the phenyl radical and/or benzene via the self-reaction of two propargyl radicals.<sup>5,7,16</sup>

Received: October 12, 2010

Revised: December 6, 2010

Published: December 31, 2010

Whereas significant experimental and theoretical work has been conducted on the formation,<sup>17,18</sup> unimolecular decomposition,<sup>19,20</sup> and reactivity of the propargyl radical<sup>1,4,7,21–25</sup> ( $\text{H}_2\text{CCCH}$ ; hereafter:  $\text{C}_3\text{H}_3$ ), comparatively little research has been carried out on the next higher member of this series: resonantly stabilized  $\text{C}_5\text{H}_3$  isomers, among them the  $\text{C}_{2v}$  symmetric 2,4-pentadiynyl-1 radical ( $\text{H}_2\text{CCCCCH}$ ).<sup>26,27</sup> This radical is of a similar importance when compared to propargyl since theoretical studies showed that the incorporation of one additional carbon–carbon triple bond in the delocalized system only marginally decreases the stabilization energy.<sup>28</sup> It should be noted that three isomers of the  $\text{C}_5\text{H}_3$  radical were suggested to be present in fuel-rich flames as elucidated via photoionization mass spectrometry using bright synchrotron radiation: *i*- $\text{C}_5\text{H}_3$  ( $\text{H}_2\text{CCCCCH}$ ), *n*- $\text{C}_5\text{H}_3$  ( $\text{HCCCHCCH}$ ), and *cyclo*- $\text{C}_5\text{H}_3$  at a ratio of 9:3:1, respectively.<sup>26</sup> From 25 isomeric forms of the  $\text{C}_5\text{H}_3$  radical, Mebel and co-workers<sup>29</sup> confirmed by electronic structure calculations that these three radicals hold the lowest enthalpies of formation. The acyclic *i*- and *n*- $\text{C}_5\text{H}_3$  isomers are about  $130 \text{ kJ mol}^{-1}$  more stable than the cyclic isomer with the *i*- $\text{C}_5\text{H}_3$  isomer stabilized by about  $3 \text{ kJ mol}^{-1}$  compared to the *n*- $\text{C}_5\text{H}_3$  structure. Both acyclic radicals have  $\text{C}_{2v}$  symmetry and a  $^2\text{B}_1$  electronic ground state. Laboratory experiments under collision-free conditions and computations suggested various pathways by which the  $\text{C}_5\text{H}_3$  isomers could be formed under combustion-like conditions. First, the formation of  $\text{C}_5\text{H}_3$  and the methyl radical ( $\text{CH}_3$ ) was an open channel in the photodissociation of benzene both experimentally<sup>30</sup> and theoretically.<sup>29,31</sup> Second, crossed molecular beam experiments of dicarbon molecules with methylacetylene ( $\text{CH}_3\text{CCH}$ ) and allene ( $\text{H}_2\text{CCCH}_2$ ) on the singlet and triplet manifolds suggested the formation of the 2,4-pentadiynyl-1 radical (*i*- $\text{C}_5\text{H}_3$ ;  $\text{H}_2\text{CCCCCH}$ )<sup>32</sup> via indirect scattering dynamics (reaction (1)). By using D3-methylacetylene, it was possible to determine that the hydrogen loss originated from the methyl group rather than the acetylenic section of the molecule. The reaction of dicarbon with allene, however, was suggested to lead to two distinct isomers: the 2,4-pentadiynyl-1 radical (*i*- $\text{C}_5\text{H}_3$ ;  $\text{H}_2\text{CCCCCH}$ ) and the 1,4-pentadiynyl-1 radical (*n*- $\text{C}_5\text{H}_3$ ;  $\text{HCCCHCCH}$ ) (reaction (2)) on triplet and singlet surfaces.<sup>33</sup> Finally, the reaction of tricarbon with ethylene ( $\text{H}_2\text{CCH}_2$ ) as conducted under single collision conditions lead via atomic hydrogen loss to the 2,4-pentadiynyl-1 radical<sup>34</sup> (*i*- $\text{C}_5\text{H}_3$ ;  $\text{H}_2\text{CCCCCH}$ ) (reaction (3)), (term symbols are omitted for clarity).



Considering that both the  $\text{C}_2/\text{C}_3\text{H}_4$  and  $\text{C}_3/\text{C}_2\text{H}_4$  systems access the  $\text{C}_5\text{H}_4$  potential energy surfaces, it is logical to conclude that the reaction of ground state carbon atoms,  $\text{C}(^3\text{P}_j)$ , with  $\text{C}_4\text{H}_4$  isomers shall also proceed on the triplet  $\text{C}_5\text{H}_4$  potential energy surface. Among the  $\text{C}_4\text{H}_4$  isomers, the thermodynamically most stable vinylacetylene ( $\text{HCCC}_2\text{H}_3$ ) molecule has been detected in hydrocarbon flames.<sup>22,35,36</sup> Therefore, we decided to investigate the reaction dynamics of ground state carbon atoms with vinylacetylene under single collision conditions in a crossed molecular beams setup and to combine these experiments with electronic structure calculations. Although the  $\text{C}_5\text{H}_4$  surface has been investigated previously via reactions (1)–(3), the addition of ground state carbon to either the carbon–carbon double or

**Table 1. Peak Velocities ( $v_p$ ), Speed Ratio ( $S$ ), and the Center-of-Mass Angles ( $\Theta_{\text{CM}}$ ), Together with the Nominal Collision Energies ( $E_c$ ) of Vinylacetylene, Low Energy Carbon and High Energy Carbon Molecular Beams**

	$v_p$ ( $\text{ms}^{-1}$ )	$S$	$E_c$ ( $\text{kJmol}^{-1}$ )	$\Theta_{\text{CM}}$
$\text{C}_4\text{H}_4/\text{Ar}$	$642 \pm 20$	$26.0 \pm 1.0$		
$\text{C}(^3\text{P}_j)/\text{He}$	$2055 \pm 15$	$3.8 \pm 0.2$	$18.8 \pm 0.8$	$56.0 \pm 0.5$
$\text{C}(^3\text{P}_j)/\text{He}$	$2504 \pm 48$	$3.6 \pm 0.2$	$26.4 \pm 2.4$	$51.0 \pm 0.5$

triple bond of vinylacetylene leads to triplet collision complexes highly distinct from those observed in the reactions of dicarbon with methylacetylene/allene and of tricarbon with ethylene. Therefore, the current investigation will lead to a systematic understanding of discrete parts of the  $\text{C}_5\text{H}_4$  surface—both from the experimental and theoretical viewpoints—and can be placed within the context of the dicarbon–allene/methylacetylene and tricarbon–ethylene systems studied earlier. The dynamics of the carbon–vinylacetylene reaction ( $\text{C}_5\text{H}_4$  PES) are then compared with related reactions of ground state carbon atoms with the individual building blocks of vinylacetylene, i.e., ethylene ( $\text{C}_2\text{H}_4$ )<sup>18,37</sup> and acetylene ( $\text{C}_2\text{H}_2$ ).<sup>38</sup>

## 2. EXPERIMENTAL AND DATA ANALYSIS

The experiments were carried out under single collision conditions in a crossed molecular beams machine at the University of Hawaii.<sup>39</sup> Briefly, a supersonic beam of ground state carbon atoms,  $\text{C}(^3\text{P}_j)$ , was produced by laser ablation of a rotating carbon rod<sup>40</sup> by focusing the fourth harmonic of a Spectra-Physics Quanta-Ray Pro 270 Nd:YAG laser operating at 266 nm and 30 Hz onto the rod at a peak power of 4–7 mJ per pulse. The distance between the nozzle and the skimmer was 36 mm. The rotating carbon rod was mounted on a homemade ablation source.<sup>40</sup> The ablated species as generated in the primary source region of the chamber was seeded in a pulsed helium carrier gas (99.9999%, Airgas) at a backing pressure of 4 atm from a Proch-Trickl pulsed valve operated at repetition rates of 60 Hz, amplitudes of  $-450 \text{ V}$  and opening times of  $75 \mu\text{s}$ . Under these operating conditions, the pressure in the primary source was maintained at  $4 \times 10^{-4}$  Torr. The molecular beam passed a skimmer and a four-slot chopper wheel, which selected a segment of the pulsed carbon beam of a well-defined peak velocity ( $v_p$ ) and speed ratio ( $S$ ). Experiments were conducted with two different segments of the beam. These are characterized by a low velocity,  $v_p = 2055 \pm 15 \text{ ms}^{-1}$ ,  $S = 3.8 \pm 0.23$ , and a high velocity of  $v_p = 2504 \pm 48 \text{ ms}^{-1}$  and  $S = 3.6 \pm 0.21$  (Table 1). The carbon beam perpendicularly bisects a pulsed beam of 5% argon-seeded vinylacetylene ( $\text{C}_4\text{H}_4$ ) released by a second pulsed valve at 550 Torr with a peak velocity  $v_p = 642 \pm 20 \text{ ms}^{-1}$  and speed ratio,  $S = 26 \pm 1$  (Table 1); argon was obtained from BOC Gases, 99.9999% purity; vinylacetylene was synthesized in our laboratory as described in an earlier work to a purity of 99.5% or higher.<sup>41</sup> The secondary pulsed valve was operated at repetition rates of 60 Hz, amplitudes of minus 500 V, and opening times of  $80 \mu\text{s}$ . The chopper wheel defined the time zero in the experiments. Assisted by two frequency dividers (Pulse Research Lab, PRL-220A) and three pulse generators (Stanford Research System, DG535), a photodiode mounted on top of the chopper wheel provided the time zero trigger to control the experiment. The primary pulsed valve opened 1860 and  $1862 \mu\text{s}$  after  $t = 0$ , and the secondary pulsed valve opened 1846 and  $1844 \mu\text{s}$  after  $t = 0$  for the low and high velocity experiments,

respectively. The collision energies were  $18.8 \pm 0.8 \text{ kJ mol}^{-1}$  and  $26.4 \pm 2.4 \text{ kJ mol}^{-1}$  for the low and high velocities, respectively. It should be noted that laser ablation of the carbon rod produces dicarbon and tricarbon molecules as well.<sup>42</sup> Signal from tricarbon can fundamentally be discarded since the collision energies used are below the  $50 \text{ kJ mol}^{-1}$  required to achieve reaction.<sup>42</sup> The production of carbon is maximized compared to dicarbon through the position of the laser beam on the carbon rod and the segment of the primary beam selected by the chopper wheel to give rise to an angular distribution with no mass interference from the dicarbon reaction with vinylacetylene. We achieve relative ratios for carbon and dicarbon in the beam of 1:0.01, respectively, for both collision energies.

The reaction products were monitored using a triply differentially pumped quadrupole mass spectrometer (QMS) in the time-of-flight (TOF) mode after electron-impact ionization of the neutral molecules at 80 eV at an emission current of 2 mA. These charged particles were then separated according to mass to charge ratio by an Extrel QC 150 quadrupole mass spectrometer operated with an oscillator at 2.1 MHz; only ions with the desired mass-to-charge,  $m/z$ , value passed through and were accelerated toward a stainless steel “door knob” target coated with an aluminum layer and operated at a voltage of  $-22.5 \text{ kV}$ . The ions hit the surface and initiated an electron cascade that was accelerated by the same potential until they reached an aluminum coated organic scintillator whose photon cascade was detected by a photomultiplier tube (PMT, Burle, Model 8850, operated at  $-1.35 \text{ kV}$ ). The signal from the PMT was then filtered by a discriminator (Advanced Research Instruments, Model F-100TD, level:  $1.4 \text{ mV}$ ) prior to feeding into a Stanford Research System SR430 multichannel scaler to record time-of-flight spectra.<sup>43,44</sup> TOF spectra were recorded at  $2.5^\circ$  intervals over the angular distribution. Up to  $2.1 \times 10^4$  TOF spectra were recorded at each angle.

The TOF spectra at each angle and the product angular distribution in the laboratory frame (LAB) were fit with Legendre polynomials using a forward-convolution routine, which is described in detail earlier.<sup>45,46</sup> This method uses an initial choice of the product translational energy,  $P(E_T)$ , and the angular distribution,  $T(\theta)$ , in the center of mass reference frame (CM). The TOF spectra obtained from the fit are compared to the experimental data. The parameters of  $P(E_T)$  and  $T(\theta)$  are iteratively optimized until the best fit is found. The output of the fitting routine is used to create a visually intuitive representation of the chemical dynamics in the form of a contour plot. Here, the product flux contour map,  $I(\theta, u) = P(u) \times T(\theta)$ , is a plot of the intensity of the reactively scattered products ( $I$ ) as a function of the center-of-mass scattering angle ( $\theta$ ) and product velocity ( $u$ ). This plot is the reactive differential cross section and gives an image of the chemical reaction. Processing of the raw TOF spectra to averaged TOF spectra and the product angular distribution was conducted using a newly written Labview program code. This program normalizes the TOF data based on the data accumulation times and drifts in the intensity of the carbon beam.

### 3. THEORETICAL

Stationary points on the  $\text{C}_5\text{H}_4$  triplet potential energy surface (PES) accessed by the reaction of ground state carbon atoms ( $\text{C}(^3\text{P}_j)$ ) with vinylacetylene, including the reactants, intermediates, transition states, and possible products, were optimized at the hybrid density functional B3LYP level with the 6-311G\*\*

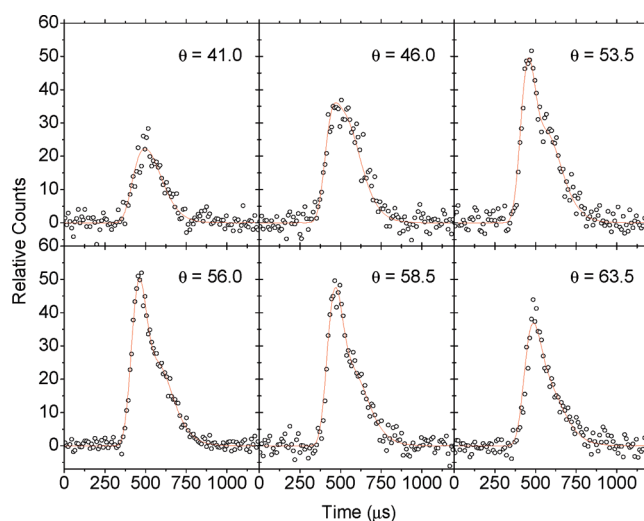


**Figure 1.** Time-of-flight data recorded at  $m/z = 63$  for the reaction of carbon and vinylacetylene at a collision energy of  $18.8 \text{ kJ mol}^{-1}$ . The circles indicate the experimental data, and the solid lines indicate the calculated fit.

basis set.<sup>47,48</sup> Vibrational frequencies were calculated using the same B3LYP/6-311G\*\* method and were used to compute zero-point vibrational energy (ZPE) corrections. Relative energies of various species were refined employing the coupled cluster CCSD(T) method<sup>49–52</sup> with extrapolation to the complete basis set (CBS) limit from total energy calculations with Dunning's correlation-consistent cc-pVDZ, cc-pVTZ, and cc-pVQZ basis sets<sup>53,54</sup> and including ZPEs obtained by B3LYP calculations. All quantum chemical calculations were performed utilizing the GAUSSIAN 98<sup>55</sup> and MOLPRO<sup>56</sup> program packages. The results of the ab initio calculations, such as relative energies and molecular parameters, were utilized in RRKM calculations of energy-dependent rate constants, which in turn were used to compute product branching ratios at different collision energies.<sup>57</sup>

### 4. EXPERIMENTAL RESULTS

Reactive scattering signal was recorded at both collision energies at  $m/z = 63$  ( $\text{C}_5\text{H}_3^+$ ),  $62$  ( $\text{C}_5\text{H}_2^+$ ), and  $64$  ( $^{13}\text{C}_4\text{H}_3^+$ ). The TOF spectra at all  $m/z$  values had the same time domain spectral profiles indicating that the spectra at  $m/z = 62$  originated from dissociative ionization of the  $\text{C}_5\text{H}_3$  parent product in the electron impact ionizer; signal at  $m/z = 64$  ( $^{13}\text{C}_4\text{H}_3^+$ ) resulted from the naturally abundant  $^{13}\text{C}$  isotope. These observations alone suggest that only the hydrogen atom loss channel is open in this mass range and that the molecular hydrogen loss channel is closed. Figures 1 and 2 depict selected TOF spectra for both collision energies. It should be noted that the fits of the TOF spectra were conducted using a single channel with a mass combination of 63 amu ( $\text{C}_5\text{H}_3$ ) and 1 amu (H). The TOF spectra at each angle were also integrated and scaled according to the number of scans to derive the laboratory angular distribution (LAB) of the  $\text{C}_5\text{H}_3$  products at the most intense  $m/z$  value of 63 ( $\text{C}_5\text{H}_3^+$ ) (Figures 3 and 4) for both energies. In the low velocity experiment, the center-of-mass angle is  $56.0^\circ \pm 0.5^\circ$ , as indicated in Figure 3. The angular distribution obtained at the higher collision energy shows a similar scenario with the center-of-mass angle calculated to be  $51.0^\circ \pm 0.5^\circ$ ; the angular distribution peaks at  $48.5^\circ \pm 0.5^\circ$ . These observations imply that the reaction likely proceeds via

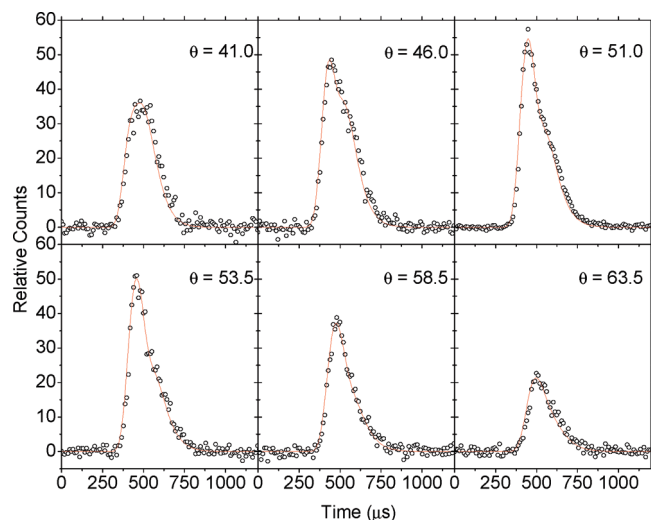


**Figure 2.** Time-of-flight data recorded at  $m/z = 63$  for the reaction of carbon and vinylacetylene at a collision energy of  $26.4 \text{ kJ mol}^{-1}$ . The circles indicate the experimental data, and the solid lines indicate the calculated fit.

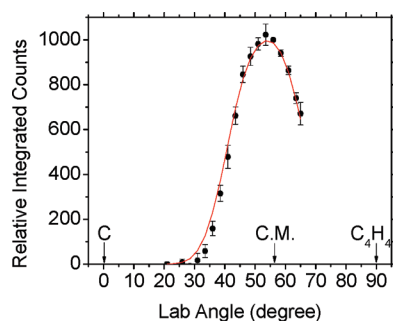


**Figure 3.** Laboratory angular distribution of the  $\text{C}_5\text{H}_3$  isomer(s) formed in the reaction of ground state carbon atoms with vinylacetylene at a collision energy of  $18.8 \text{ kJ mol}^{-1}$ . Circles and error bars indicate experimental data, and solid lines indicate calculated distribution.

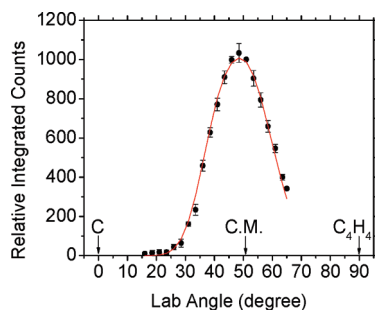


**Figure 4.** Laboratory angular distribution of the  $\text{C}_5\text{H}_3$  isomer(s) formed in the reaction of ground state carbon atoms with vinylacetylene at a collision energy of  $26.4 \text{ kJ mol}^{-1}$ . Circles and error bars indicate experimental data, and solid lines indicate calculated distribution.

indirect (complex forming) scattering dynamics involving  $\text{C}_5\text{H}_4$  reaction intermediate(s).

Having interpreted the laboratory data, we are turning our attention now to the corresponding center-of-mass functions. From the center-of-mass translational energy distribution,  $P(E_T)$ , best fits of the laboratory data of the lower and higher collision

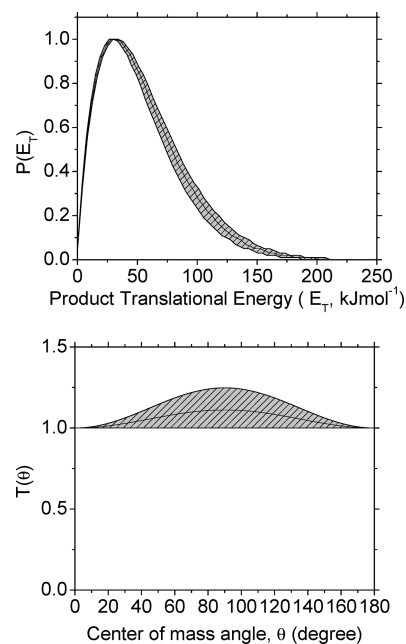


**Figure 5.** Center-of-mass translational energy distribution (top) and center-of-mass angular distribution (bottom) for the reaction of carbon with vinylacetylene to form the  $\text{C}_5\text{H}_3$  radical(s) and atomic hydrogen at a collision energy of  $18.8 \text{ kJ mol}^{-1}$ .

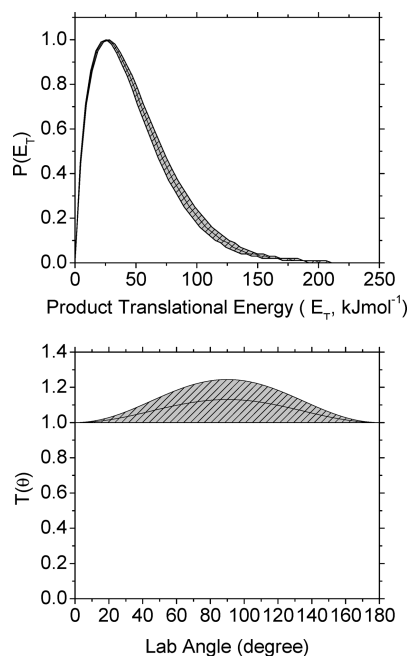


**Figure 6.** Center-of-mass translational energy distribution (top) and center-of-mass angular distribution (bottom) for the reaction of carbon with vinylacetylene to form the  $\text{C}_5\text{H}_3$  radical(s) and atomic hydrogen at a collision energy of  $26.4 \text{ kJ mol}^{-1}$ .

energy were achieved with single channel fits extending to maximum translational energy releases of  $188 \pm 16 \text{ kJ mol}^{-1}$  and  $196 \pm 10 \text{ kJ mol}^{-1}$ , respectively (Figures 5 (top) and 6 (top)). Since the maximum energy released is equivalent to the sum of the reaction exoergicity and the collision energy due to energy conservation, we can subtract the latter to extract the experimentally determined reaction exoergicity forming the  $\text{C}_5\text{H}_3$  isomer(s)

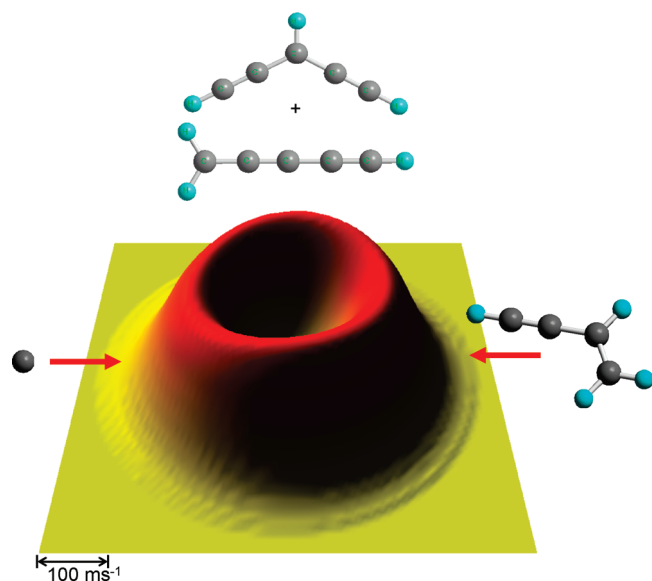


**Figure 7.** Flux contour map of the reaction of carbon with vinylacetylene to form  $C_5H_3$  radical(s) and atomic hydrogen at a collision energy of  $18.8 \text{ kJ mol}^{-1}$ .

plus atomic hydrogen to be  $171 \text{ kJ mol}^{-1}$  and  $169 \text{ kJ mol}^{-1}$ , for the low and high collision energies, respectively. It should be noted that in the present system, the tail can be cut or extended by up to  $20 \text{ kJ mol}^{-1}$  without changing the quality of the fit. Therefore, the experiments suggest that the formation of the  $C_5H_3$  isomers is exoergic by  $170 \pm 36 \text{ kJ mol}^{-1}$ . Also, as can be seen from the  $P(E_T)$ s, the flux distributions peak away from zero translational energy. This indicates that at least one reaction channel to form the  $C_5H_3$  isomer(s) has a tight exit transition state (repulsive carbon–hydrogen bond rupture involving a significant electron rearrangement). The center-of-mass translational energy distributions allow us to determine the amount of energy released into the translational degrees of freedom of the products to be  $49 \pm 5 \text{ kJ mol}^{-1}$  for the low velocity (25% of the total available internal energy). For the high velocity,  $51 \pm 5 \text{ kJ mol}^{-1}$  is released as translational energy (27% of the total available internal energy). A comparison of these data with related complex-forming reactions of ground state carbon atoms<sup>58,59</sup> suggests that the reaction proceeds in an indirect fashion via complex formation.

The center-of-mass angular distribution  $T(\theta)$  at the lower and higher collision energies as shown in Figures 5 and 6 depict a forward–backward symmetric distribution over the full angular range. This is indicative of an indirect, complex-forming reaction mechanism, in which the lifetime of the decomposing reaction intermediate(s) is/are longer than the rotational period. Figures 7 and 8 show the corresponding center-of-mass flux contour maps for the low and high velocities. Both figures clearly display forward–backward symmetric distributions over their full angular ranges. It should be noted that the data could be fit with isotropic distributions, but also with functions in which the  $T(\theta)$ s depict a slight maximum at  $90^\circ$  (sideways scattering). For the isotropic fits, these results show a weakly polarized system suggesting that the initial orbital angular momentum does not couple well to the final orbital angular momentum due to the light mass of the departing hydrogen atom; further, most of the initial angular momentum is channeled into the rotational degrees of freedom of the  $C_5H_3$  product isomer(s).<sup>60</sup> In case of the sideways

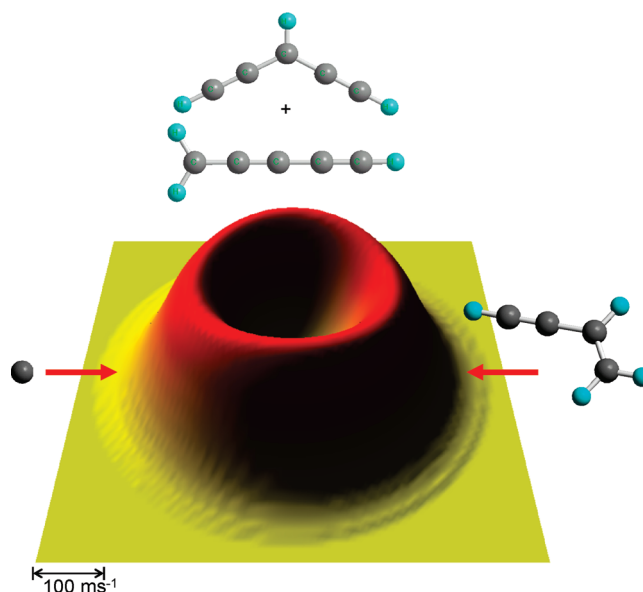


**Figure 8.** Flux contour map of the reaction of carbon with vinylacetylene to form  $C_5H_3$  radical(s) and atomic hydrogen at a collision energy of  $26.4 \text{ kJ mol}^{-1}$ .

scattering, this shape of the center-of-mass angular distribution suggests geometrical constraints when the decomposing complex emits a hydrogen atom parallel to the total angular momentum vector.

## 5. THEORETICAL RESULTS

The experimental results from the cross beam apparatus were complemented by electronic structure calculations to characterize the pertinent part of the triplet  $C_5H_4$  potential energy surface (PES) (Figure 9). The initial reaction of atomic carbon ( $C(^3P_j)$ ) with vinylacetylene ( $C_3H_3(X^1A')$ ) can proceed via two pathways. The first pathway involves the carbon atom adding to the  $\pi$  electron density of the carbon–carbon triple bond of the vinylacetylene molecule to form a cyclic intermediate, **i1**, with  $C_s(X^3A'')$  symmetry and an exoergicity of  $253 \text{ kJ mol}^{-1}$ . This intermediate then overcomes a barrier of only  $29 \text{ kJ mol}^{-1}$  through ring-opening to isomerize to the lowest energy intermediate, **i2**, stabilized by  $409 \text{ kJ mol}^{-1}$ ; both **i1** and **i2** have identical symmetries and electronic ground states. The second pathway involves the carbon atom attacking the  $\pi$  electron density of the carbon–carbon double bond of vinylacetylene forming a cyclic intermediate, **i3**, with  $C_1(X^3A)$  symmetry. This structure is energetically less stable ( $-216 \text{ kJ mol}^{-1}$ ) compared to **i1**. From **i3**, the molecular ring opens via a barrier of  $41 \text{ kJ mol}^{-1}$  to access a local minima, **i4**, stabilized by  $362 \text{ kJ mol}^{-1}$ ; this structure has a  $C_s(X^3A'')$  symmetry. This intermediate can also be accessed from **i2** via hydrogen atom migration by overcoming a significant barrier of  $246 \text{ kJ mol}^{-1}$ . From **i2**,  $i-C_5H_3$  ( $H_2CCCCCH$ ) can be formed in an overall exoergic reaction ( $-212 \text{ kJ mol}^{-1}$ ) via atomic hydrogen loss from the central carbon atom via a tight exit transition state located  $13 \text{ kJ mol}^{-1}$  above the separated products. This isomer ( $i-C_5H_3$ ) is also accessed from **i4** via a transition state located  $28 \text{ kJ mol}^{-1}$  above the separated products. Intermediate **i5**, bound by  $361 \text{ kJ mol}^{-1}$ , can be accessed from **i4** via another hydrogen shift by overcoming a significant energy barrier of  $202 \text{ kJ mol}^{-1}$ .

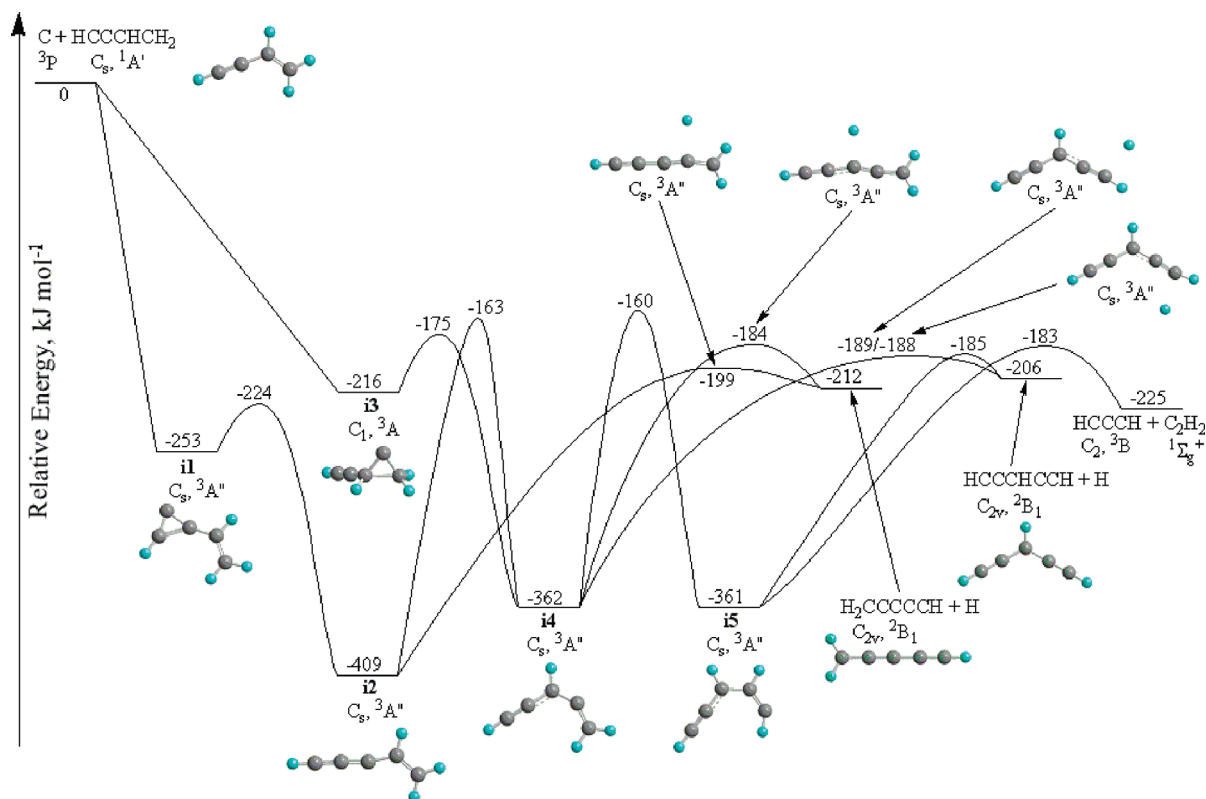


**Figure 9.** Potential energy surfaces (PESs) of the reaction of ground-state carbon atom with vinylacetylene to form the  $C_5H_3$  radical(s) plus atomic hydrogen. Energies are given in  $\text{kJ mol}^{-1}$ .

The second product isomer,  $n$ - $C_5H_3$  (HCCCHCCH), can be formed in an overall exoergic ( $-206 \text{ kJ mol}^{-1}$ ) via intermediate **i4** through a transition state located about  $18 \text{ kJ mol}^{-1}$  above the final products. This isomer is also accessible from **i5** via a tight exit transition state located  $21 \text{ kJ mol}^{-1}$  above the products. Note that intermediate **i5** can also fragment to propargylene (HCCCH;  $C_2$ ,  $X^3B$ ) and acetylene ( $C_2H_2$ ;  $X^1\Sigma_g^+$ ) in an exoergic reaction ( $-225 \text{ kJ mol}^{-1}$ ). Note also that in analogy to the carbon–acetylene reaction, we investigated the structure resulting from an attack of the carbon atom to the terminal carbon atom of the carbon–carbon triple bond of vinylacetylene. At the B3LYP level, this results in a local minimum **i0**. The barriers for cyclization (**i0**–**i1**) and hydrogen shift (**i0**–**i2**) are  $3.3$  and  $9.2 \text{ kJ mol}^{-1}$ , respectively. At the higher level of theory at the CCSD(T)/CBS level, **i0** was found to have a transition state to **i1**  $2.9 \text{ kJ mol}^{-1}$  lower in energy than **i0** itself implying **i0** cannot be regarded as a local minimum. If **i0** were to be accessed, then it would rapidly rearrange to **i1** and only exist as a metastable structure and so is not included in the reaction pathways as depicted in Figure 9. Finally, the addition of ground state carbon to the C2 atom in vinylacetylene, i.e., the second carbon atom located in the carbon–carbon triple bond, does not result in a local minimum either. To summarize, the electronic structure calculations alone suggest that both  $C_5H_3$  isomers ( $n$ - and  $i$ - $C_5H_3$ ) can be formed in the reaction of ground state carbon atoms with vinylacetylene.

The actual product branching ratio between  $n$ - $C_5H_3$  and  $i$ - $C_5H_3$  is very sensitive to the initial branching ratio of **i1** versus **i3**, i.e., the addition of carbon atoms to the carbon–carbon triple versus double bond (Table 2). Here, starting from **i1**, we find that  $i$ - $C_5H_3$  is formed almost exclusively. This can be rationalized

**Table 2.** RRKM Calculated Product Branching Ratios (%) at Different Collision Energies Assuming a One to One Entrance Channel Branching Ratio toward **i1**/**i3** Initial Intermediates

products	$E_c$ , $\text{kJ mol}^{-1}$		
	0.0	18.8	26.4
$i$ - $C_5H_3$ from <b>i2</b>	51.1	51.0	51.0
$i$ - $C_5H_3$ from <b>i4</b>	8.2	8.4	8.4
$i$ - $C_5H_3$ total	59.3	59.4	59.4
$n$ - $C_5H_3$ from <b>i4</b>	39.9	39.6	39.5
$n$ - $C_5H_3$ from <b>i5</b>	0.2	0.2	0.2
$n$ - $C_5H_3$ total	40.1	39.8	39.7
HCCCH + $C_2H_2$	0.6	0.8	0.9

considering the barrier involved in the decomposition of **i2** to  $i$ - $C_5H_3$  plus atomic hydrogen located at  $-199 \text{ kJ mol}^{-1}$  compared to the barrier required for **i2** to isomerize to **i4** ( $-163 \text{ kJ mol}^{-1}$ ). Recall that based on the PES, only  $i$ - $C_5H_3$  can be formed from **i2** whereas to yield  $n$ - $C_5H_3$ , **i2** has to isomerize first to **i4**, however, starting from **i3**, formation of  $n$ - $C_5H_3$  is preferable (Table 2). These two reaction pathways are analogous to the reactions between carbon atoms with acetylene and ethylene. Utilizing ratios of the rate constants of the reactions of carbon atoms with acetylene and ethylene in the order of one for the initial branching ratio of **i1** versus **i3** as measured by Sims et al.,<sup>61</sup> we find a ratio of  $n$ - $C_5H_3$  to  $i$ - $C_5H_3$  of about 2:3; within the error limits, this ratio is invariant with the collision energy of the crossed beam reactions. Note the initial branching ratio has been selected for simplicity but with acknowledgment that the reaction dynamics

between a unitary and conjugated bonding system are different. In the special case of vinylacetylene, the bonding is known to be highly localized so the present analogy is appropriate.<sup>62,63</sup> Further, the ratio between the rates of reaction of atomic carbon with alkenes compared with dienes, and alkynes compared with diynes shows that the rates between unitary and multiple double or triple bonds vary but that the differences in ratios between the double and triple bond species are negligible.<sup>64</sup> The rates of reaction for each step in the reaction paths which were used to derive the branching ratios have been added in the Supporting Information.

## 6. DISCUSSION

In order to elucidate the reaction pathway between the ground state carbon atom,  $C(^3P_1)$ , and vinylacetylene we combined cross molecular beams experiments at two collision energies of  $18.8 \pm 0.8 \text{ kJ mol}^{-1}$  and  $26.4 \pm 2.4 \text{ kJ mol}^{-1}$  with electronic structure calculations of the triplet  $C_5H_4$  potential energy surface. First, based on the center-of-mass angular distributions, the experiments showed that for both collision energies, the reaction to form  $C_5H_3$  isomers as detected at  $m/z = 63$  ( $C_5H_3^+$ ) proceeded via indirect scattering dynamics involving  $C_5H_4$  collision complexes. This has been verified by the electronic structure calculations as the reactions to form  $n-C_5H_3$  and/or  $i-C_5H_3$  are initiated by a barrierless addition of the carbon atom forming **i1** and/or **i3**. Also, the fraction of energy of 25–27% channeling into the translational degrees of freedom is indicative of an indirect reaction mechanism. Consequently, both experiment and theory correlate well. Second, the theoretical calculations could not predict any reaction pathway leading to the formation of molecular hydrogen. Again, this is in excellent agreement with our experiments, since only an atomic hydrogen loss was observable. Third, the center-of-mass translational energy distributions suggested a tight exit transition state upon decomposition of the triplet  $C_5H_4$  intermediate(s) to  $n-C_5H_3$  and/or  $i-C_5H_3$ . This could be verified theoretically as all four feasible reaction pathways (**i2/i4**  $\rightarrow$   $i-C_5H_3$ ; **i4/i5**  $\rightarrow$   $n-C_5H_3$ ) involved tight exit transition states via barriers between 13 to  $28 \text{ kJ mol}^{-1}$ .

We are now finally attempting to answer which  $C_5H_3$  isomer is formed in the reaction. The experiments suggest an exoergicity of  $170 \pm 36 \text{ kJ mol}^{-1}$ . A comparison with both computed reaction exoergicities leading to  $n-C_5H_3$  and  $i-C_5H_3$  of 206 and  $212 \text{ kJ mol}^{-1}$  does not reveal the nature of the isomer based on the reaction energy alone. Also, the agreement of the experiments with theory is not as good as expected in related reactions of carbon atoms with acetylene<sup>38,65</sup> and ethylene,<sup>18,37</sup> suggesting that the final reaction products are highly internally excited. This was verified by the low fraction of energy of only 25–27% channeling into the translational degrees of freedom of the reaction products.

The only experimental indication of isomer preference comes from the center-of-mass angular distribution. We can see from the two transition state structures leading to  $i-C_5H_3$  in Figure 9 that there is a preferential hydrogen loss direction perpendicular to the principal rotation axis of the molecule. According to micro-canonical theory, if  $\beta$ , the angle between the exiting hydrogen atom and the primary rotation axis,  $A$ , is  $90^\circ$  for a prolate linear rotor, then the center-of-mass angular distribution will show sideways scattering.<sup>66</sup> This is the case for  $i-C_5H_3$ , whereas for  $n-C_5H_3$  the exiting hydrogen atom has a value for  $\beta$  in the  $30^\circ$ – $60^\circ$  range resulting in a broader/isotropic center-of-mass angular distribution. Therefore, given that the center-of-mass angular

distribution is sideways scattered, we can suggest that the  $i-C_5H_3$  isomer is the predominant product, and, since the center-of-mass angular distribution can be fit with an isotropic distribution within the errors limit the  $n-C_5H_3$  isomer is also being formed to a lesser extent. On the basis of the calculations, the critical points of the potential energy surface along with an initial branching ratio of unity (based on the ratio of the rate constants for the related reactions of ground state carbon atoms with acetylene)<sup>61</sup> imply that the formation of  $i-C_5H_3$  or  $n-C_5H_3$  are likely formed with a ratio of three to two—independent of the collision energy (Table 2). The initial branching ratio plays the most important role in determining the outcome of the reaction, in which **i1** almost entirely leads to  $i-C_5H_3$  and **i3** predominantly leads to  $n-C_5H_3$ . This is dependent on whether the carbon atom attacks the double bond (similar to the reaction with ethylene<sup>18,37</sup>) or the triple bond (similar to the reaction with acetylene<sup>38</sup>) of vinylacetylene.

The reaction pathway from **i1** to  $i-C_5H_3$  starts with the carbon atom attacking the  $\pi$  electron density of the triple bond of vinylacetylene. This reaction can be compared to the pathways available in the reaction of atomic carbon with acetylene ( $C_2H_2$ )<sup>38</sup> which has been investigated using the same experimental setup and over a range of collision energies from 8– $31 \text{ kJ mol}^{-1}$ . The first step in this reaction is the formation of a cyclic intermediate which possesses a similar structure and relative energy of  $-215 \text{ kJ mol}^{-1}$  ( $38 \text{ kJ mol}^{-1}$  higher than **i1**) to the first intermediate, **i1**, in the vinylacetylene reaction. The cyclic intermediate, **i1**, ring opens to a bent structure, **i2**, representing the global minimum of the PES. The reaction of atomic carbon with acetylene also holds similar features, and the initial cyclic addition product opens to the triplet propargylene intermediate (HCCCCH) stabilized by  $388 \text{ kJ mol}^{-1}$  with respect to the reactants. From **i2**, a hydrogen loss yields the  $i-C_5H_3$  product. Interestingly, the reaction of atomic carbon with acetylene was also found to form singlet tricarbon ( $C_3$ ) plus molecular hydrogen ( $H_2$ ) potential involving intersystem crossing.<sup>38,67</sup> This reaction pathway becomes accessible as the lifetime of the complex increases. Our experimental findings indicate that the reaction pathway to form molecular hydrogen and any isomer at  $m/z = 50$  ( $C_3H_2^+$ ) was closed; therefore, it is likely that ISC does not play a role in the atomic carbon–vinylacetylene system.

The second micro channel in the reaction of atomic carbon with vinylacetylene is from **i3** to  $n-C_5H_3$  and involves atomic carbon attacking the  $\pi$  electron density of the double bond. This reaction pathway can be compared to the attack of a carbon atom on the double bond of ethylene, ( $C_2H_4$ ).<sup>18,37</sup> The cyclic intermediate **i3** is the first step in the reaction pathway to  $n-C_5H_3$  which possesses the same structure and relative energy ( $1 \text{ kJ mol}^{-1}$  higher) as the first intermediate, cyclopropylidene, in the reaction of atomic carbon with ethylene. From **i3**, **i4** is reached, which has a triplet allenic structure. The atomic carbon with ethylene reaction reaches a similar structural intermediate in its second step with  $-343 \text{ kJ mol}^{-1}$  of energy relative to the reactants which is  $20 \text{ kJ mol}^{-1}$  less. The complex moves between these two structures via a transition state with a relative energy of  $-160 \text{ kJ mol}^{-1}$  that is  $15 \text{ kJ mol}^{-1}$  lower in energy than the corresponding  $C_5H_4$  structure. The bent  $n-C_5H_3$  product is accessed from **i4** after hydrogen loss from the terminal carbon and subsequent electron rearrangement. The ethylene reaction product analog has a relative energy of  $-190 \text{ kJ mol}^{-1}$  ( $15 \text{ kJ mol}^{-1}$  lower than  $n-C_5H_3$ ), and is accessed via a transition state with a relative energy of  $-171 \text{ kJ mol}^{-1}$ ,  $15 \text{ kJ mol}^{-1}$  less than its  $C_5H_4$

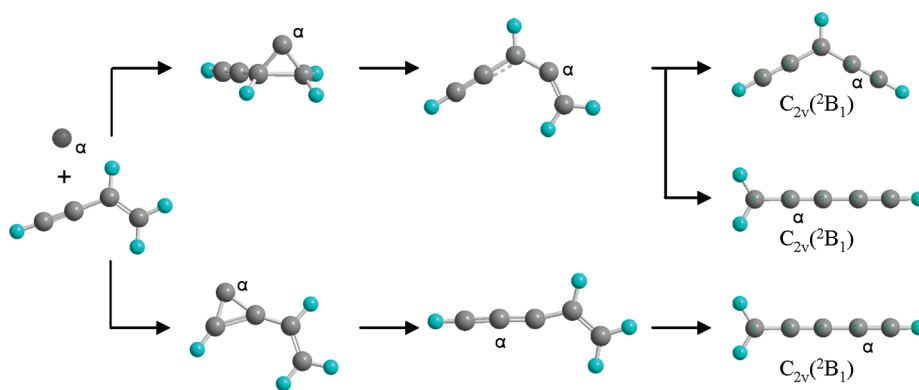


**Figure 10.** Schematic representation of the reaction pathways in the reaction of ground-state carbon with vinylacetylene to form the  $C_5H_3$  radicals and the positions of the formally “inserted” carbon atom in the final reaction products.

counterparts. In summary, the topology of vinylacetylene potential energy surface, and its reaction dynamics, show marked similarities, for the triple bond attack to acetylene and for the double bond attack to ethylene.

Let us consider where the attacking carbon atom will be incorporated in the carbon chain of  $C_5H_3$  as shown in Figure 10; the attacking carbon atom has been labeled  $\alpha$  for clarity. The first step in the top reaction pathway in Figure 10 results from addition of the carbon atom to the double bond, to form a cyclic intermediate, **i3**. The ring structure opens as the attacking carbon atom forces the double bond apart leaving itself as the second carbon in the chain, **i4**. The final step in this process is hydrogen elimination, which happens either from the terminal  $CH_2$  group to produce the bent  $n$ - $C_5H_3$  radical (1) or from the middle carbon to form the linear  $i$ - $C_5H_3$  radical (2). The second area the carbon atom will attack is the triple bond of vinylacetylene as shown in the bottom of Figure 10. Similarly, a triatomic ring structure is formed, **i1**, which opens to leave the carbon in the middle of the chain, **i2**. From here, hydrogen elimination can occur only from the hydrogen on the second carbon atom, to produce the linear  $i$ - $C_5H_3$  radical (3). It should be noted that structures (2) and (3) differ distinctly by where the labeled atom resides in the carbon chain.

## 7. CONCLUSIONS

The reaction of ground state carbon atoms,  $C(^3P_1)$ , with vinylacetylene was studied at two collision energies of  $18.8 \pm 0.8$  kJ mol $^{-1}$  and  $26.4 \pm 2.4$  kJ mol $^{-1}$  employing the crossed molecular beam technique. Our experiments were combined with ab initio and RRKM calculations. The reaction has no entrance barrier and is governed by indirect scattering dynamics to form a long-lived triplet collision complex,  $C_5H_4$ . The products,  $n$ - and  $i$ - $C_5H_3$  isomers, are reached by atomic hydrogen elimination through a tight exit transition state. The reaction pathway taken is dependent on whether the carbon atom attacks the  $\pi$  electron density of the double or triple bond of vinylacetylene, to get to the products,  $n$ - and  $i$ - $C_5H_3$ , respectively. These reactions are analogous to the reaction of atomic carbon with ethylene for the double bond attack and acetylene for the triple bond attack. The electronic structure/statistical theory calculations determined the product branching ratio to be 2:3 between the  $n$ - and  $i$ - $C_5H_3$  isomers, respectively.

## ■ ASSOCIATED CONTENT

**S** Supporting Information. Rate constants ( $s^{-1}$ ) for various unimolecular reaction steps for isomerization and dissociation of

$C_5H_4$  intermediates involved in the  $C(^3P) +$  vinylacetylene reaction, calculated using RRKM theory under single-collision conditions at collision energies of 0–26.4 kJ mol $^{-1}$  (Table S1). This information is available free of charge via the Internet at <http://pubs.acs.org>.

## ■ AUTHOR INFORMATION

### Corresponding Author

\*E-mail: [ralfk@hawaii.edu](mailto:ralfk@hawaii.edu).

## ■ ACKNOWLEDGMENT

This project was supported by the U.S. Department of Energy Office of Science (DE-FG02-03-ER15411 to R.I.K. and DE-FG02-04-ER15570 to A.M.M.).

## ■ REFERENCES

- (1) Harding, L. B.; Klippenstein, S. J.; Georgievskii, Y. J. *Phys. Chem. A* **2007**, *111*, 3789.
- (2) Hansen, N.; Kasper, T.; Klippenstein, S. J.; Westmoreland, P. R.; Law, M. E.; Taatjes, C. A.; Kohse-Hoeinghaus, K.; Wang, J.; Cool, T. A. *J. Phys. Chem. A* **2007**, *111*, 4081.
- (3) Miller, J. A. *Symposium (International) on Combustion, [Proceedings]* **1996**, *26th*, 461.
- (4) Hahn, D. K.; Klippenstein, S. J.; Miller, J. A. *Faraday Discuss.* **2001**, *79*.
- (5) Richter, H.; Howard, J. B. *Phys. Chem. Chem. Phys.* **2002**, *4*, 2038.
- (6) Frenklach, M. *Phys. Chem. Chem. Phys.* **2002**, *4*, 2028.
- (7) Frenklach, M.; Yuan, T.; Ramachandra, M. K. *Energy Fuels* **1988**, *2*, 462.
- (8) Denissenko, M. F.; Pao, A.; Tang, M.-s.; Pfeifer, G. P. *Science (Washington, D. C.)* **1996**, *274*, 430.
- (9) Baird, W. M.; Hooven, L. A.; Mahadevan, B. *Environ. Mol. Mutagen* **2005**, *45*, 106.
- (10) Finlayson-Pitts, B. J.; Pitts, J. N., Jr. *Science* **1997**, *276*, 1045.
- (11) Doty, S. D.; Leung, C. M. *Astrophys. J.* **1998**, *502*, 898.
- (12) Woods, P. M.; Millar, T. J.; Herbst, E.; Zijlstra, A. A. *Astron. Astrophys.* **2003**, *402*, 189.
- (13) Trainer, M. G.; Pavlov, A. A.; Jimenez, J. L.; McKay, C. P.; Worsnop, D. R.; Toon, O. B.; Tolbert, M. A. *Geophys. Res. Lett.* **2004**, *31*, L17S08/1.
- (14) Wilson, E. H.; Atreya, S. K. *Planet. Space Sci.* **2003**, *51*, 1017.
- (15) Huang, C.; Zhang, F.; Kaiser, R. I.; Kislov, V. V.; Mebel, A. M.; Silva, R.; Gichuhi, W. K.; Suits, A. G. *Astrophys. J.* **2010**, *714*, 1249.
- (16) Miller, J. A.; Pilling, M. J.; Troe, J. *Proc. Combust. Inst.* **2005**, *30*, 43.
- (17) Blitz, M. A.; Beasley, M. S.; Pilling, M. J.; Robertson, S. H. *Phys. Chem. Chem. Phys.* **2000**, *2*, 805.

- (18) Kaiser, R. I.; Lee, Y. T.; Suits, A. G. *J. Chem. Phys.* **1996**, *105*, 8705.
- (19) Zheng, X.; Song, Y.; Zhang, J. *J. Phys. Chem. A* **2009**, *113*, 4604.
- (20) Glassman, I. *Combustion*; Academic Press: San Diego, CA, 1996.
- (21) Scherer, S.; Just, T.; Frank, P. *Proc. Combust. Inst.* **2000**, *28*, 1511.
- (22) McEnally, C. S.; Pfefferle, L. D.; Robinson, A. G.; Zwier, T. S. *Combust. Flame* **2000**, *123*, 344.
- (23) Kern, R. D.; Xie, K. *Prog. Energy Combust. Sci.* **1991**, *17*, 191.
- (24) Miller, J. A.; Klippenstein, S. J. *J. Phys. Chem. A* **2003**, *107*, 7783.
- (25) Miller, J. A.; Melius, C. F. *Combust. Flame* **1992**, *91*, 21.
- (26) Hansen, N.; Klippenstein, S. J.; Miller, J. A.; Wang, J.; Cool, T. A.; Law, M. E.; Westmoreland, P. R.; Kasper, T.; Kohse-Hoeinghaus, K. *J. Phys. Chem. A* **2006**, *110*, 4376.
- (27) Yang, B.; Huang, C.; Wei, L.; Wang, J.; Sheng, L.; Zhang, Y.; Qi, F.; Zheng, W.; Li, W.-K. *Chem. Phys. Lett.* **2006**, *423*, 321.
- (28) Rogers, D. W.; Matsunaga, N.; Zavitsas, A. A. *J. Org. Chem.* **2006**, *71*, 2214.
- (29) Mebel, A. M.; Lin, S. H.; Yang, X. M.; Lee, Y. T. *J. Phys. Chem. A* **1997**, *101*, 6781.
- (30) Yokoyama, A.; Zhao, X.; Hints, E. J.; Continetti, R. E.; Lee, Y. T. *J. Chem. Phys.* **1990**, *92*, 4222.
- (31) Pope, C. J.; Miller, J. A. *Proc. Combust. Inst.* **2000**, *28*, 1519.
- (32) Guo, Y.; Gu, X.; Balucani, N.; Kaiser, R. I. *J. Phys. Chem. A* **2006**, *110*, 6245.
- (33) Guo, Y.; Gu, X.; Zhang, F.; Mebel, A. M.; Kaiser, R. I. *J. Phys. Chem. A* **2006**, *110*, 10699.
- (34) Gu, X.; Guo, Y.; Mebel, A. M.; Kaiser, R. I. *Chem. Phys. Lett.* **2007**, *449*, 44.
- (35) Li, Y.; Zhang, L.; Tian, Z.; Yuan, T.; Zhang, K.; Yang, B.; Qi, F. *Proc. Combust. Inst.* **2009**, *32*, 1293.
- (36) Westmoreland, P. R.; Dean, A. M.; Howard, J. B.; Longwell, J. P. *J. Phys. Chem.* **1989**, *93*, 8171.
- (37) Kaiser, R. I.; Nguyen, T. L.; Le, T. N.; Mebel, A. M. *Astrophys. J.* **2001**, *561*, 858.
- (38) Gu, X.; Guo, Y.; Zhang, F.; Kaiser, R. I. *J. Phys. Chem. A* **2007**, *111*, 2980.
- (39) Gu, X.; Guo, Y.; Zhang, F.; Mebel, A. M.; Kaiser, R. I. *Faraday Discuss.* **2006**, *133*, 245.
- (40) Gu, X.; Guo, Y.; Kawamura, E.; Kaiser, R. I. *J. Vac. Sci. Technol., A* **2006**, *24*, 505.
- (41) Kim, Y. S.; Kaiser, R. I. *Astrophys. J., Suppl. Ser.* **2009**, *181*, 543.
- (42) Guo, Y.; Gu, X.; Zhang, F.; Mebel, A. M.; Kaiser, R. I. *Phys. Chem. Chem. Phys.* **2007**, *9*, 1972.
- (43) Gu, X. B.; Guo, Y.; Kawamura, E.; Kaiser, R. I. *Rev. Sci. Instrum.* **2005**, *76*, 083115/1.
- (44) Guo, Y.; Gu, X.; Kawamura, E.; Kaiser, R. I. *Rev. Sci. Instrum.* **2006**, *77*, 034701/1.
- (45) Vernon, M. Thesis, University of California, Berkeley 1981.
- (46) Weis, M. S. Ph. D. Thesis, University of California, Berkeley 1986.
- (47) Becke, A. D. *J. Chem. Phys.* **1993**, *98*, 5648.
- (48) Lee, C.; Yang, W.; Parr, R. G. *Phys. Rev. B: Condens. Matter Mater. Phys.* **1988**, *37*, 785.
- (49) Purvis, G. D., III; Bartlett, R. J. *J. Chem. Phys.* **1982**, *76*, 1910.
- (50) Scuseria, G. E.; Janssen, C. L.; Schaefer, H. F., III. *J. Chem. Phys.* **1988**, *89*, 7382.
- (51) Scuseria, G. E.; Schaefer, H. F., III. *J. Chem. Phys.* **1989**, *90*, 3700.
- (52) Pople, J. A.; Head-Gordon, M.; Raghavachari, K. *J. Chem. Phys.* **1987**, *87*, 5968.
- (53) Dunning, T. H., Jr. *J. Chem. Phys.* **1989**, *90*, 1007.
- (54) Peterson, K. A.; Dunning, T. H., Jr. *J. Phys. Chem.* **1995**, *99*, 3898.
- (55) Frisch, M. J. T., G. W.; Schlegel, H. B.; Scuseria, G. E.; Robb, M. A.; Cheeseman, J. R.; Zakrzewski, V. G.; Montgomery, J. A.; Stratmann, R. E.; Burant, J. C.; Dapprich, S.; Millam, J. M.; Daniels, R. E.; Kudin, K. N.; Strain, M. C.; Farkas, O.; Tomasi, J.; Barone, V.; Cossi, M.; Cammi, R.; Mennucci, B.; Pomelli, C.; Adamo, C.; Clifford, S.; Ochterski, J.; Petersson, G. A.; Ayala, P. Y.; Cui, Q.; Morokuma, K.; Salvador, P.; Dannenberg, J. J.; Malick, D. K.; Rabuck, A. D.; Raghavachari, K.; Foresman, J. B.; Cioslowski, J.; Ortiz, J. V.; Baboul, A. G.; Stefanov, B. B.; Liu, G.; Liashenko, A.; Piskorz, P.; Komaromi, I.; Gomperts, R.; Martin, R. L.; Fox, D. J.; Keith, T.; Al-Laham, M. A.; Peng, C. Y.; Nanayakkara, A.; Challacombe, M.; Gill, P. M. W.; Johnson, B.; Chen, W.; Wong, M. W.; Andres, J. L.; Gonzalez, C.; M. Head-Gordon, M.; Replogle, E. S.; Pople, J. A. *Gaussian 98, revision A.11*; 1998.
- (56) Amos, R. D.; Bernhardsson, A.; Berning, A.; Celani, P.; Cooper, D. L.; Deegan, M. J. O.; Dobbyn, A. J.; Eckert, F.; Hampel, C.; Hetzer, G.; Knowles, P. J.; Korona, T.; Lindh, R.; Lloyd, A. W.; McNicholas, S. J.; Manby, F. R.; Meyer, W.; Mura, M. E.; Nicklass, A.; Palmieri, P.; Pitzer, R.; Rauhut, G.; Schutz, M.; Schumann, U.; Stoll, H.; Stone, A. J.; Tarroni, R.; Thorsteinsson, T.; Werner, H.-J. *MOLPRO, version 2002.1*; 2002.
- (57) Kislov, V. V.; Nguyen, T. L.; Mebel, A. M.; Lin, S. H.; Smith, S. C. *J. Chem. Phys.* **2004**, *120*, 7008.
- (58) Kaiser, R. I. *Chem. Rev.* **2002**, *102*, 1309.
- (59) Kaiser, R. I.; Mebel, A. M. *Int. Rev. Phys. Chem.* **2002**, *21*, 307.
- (60) Levine, R. D. *Molecular Reaction Dynamics*; Cambridge University Press: Cambridge, U.K., 2005.
- (61) Chastaing, D.; James, P. L.; Sims, I. R.; Smith, I. W. M. *Phys. Chem. Chem. Phys.* **1999**, *1*, 2247.
- (62) Kim, Y. S.; Kaiser, R. I. *Astrophys. J., Suppl. Ser.* **2009**, *181*, 543.
- (63) Mebel, A. M.; Kislov, V. V.; Kaiser, R. I. *J. Chem. Phys.* **2006**, *125*, 133113/1.
- (64) Husain, D.; Ioannou, A. X. *J. Chem. Soc., Faraday Trans.* **1997**, *93*, 3625.
- (65) Kaiser, R. I.; Ochsenfeld, C.; Head-Gordon, M.; Lee, Y. T.; Suits, A. G. *J. Chem. Phys.* **1997**, *106*, 1729.
- (66) Grice, R.; Smith, D. J. *Mol. Phys.* **1993**, *80*, 1533.
- (67) Costes, M.; Daugey, N.; Naulin, C.; Bergeat, A.; Leonori, F.; Segoloni, E.; Petrucci, R.; Balucani, N.; Casavecchia, P. *Faraday Discuss.* **2006**, *133*, 157.